Nonlinear Dynamics and Global Bifurcation Phenomena in a Fixed Duty Ratio DC-DC Boost Switching Converter with a Constant Power Load

L. Benadero[a], A. El Aroudi[b,], M. Sebastiá-Rullo[b], K. Mandal[b], H. Valderrama-Blavi[b], A. Cid-Pastor[b], L. Martínez-Salamero[b]

[a]*Departament de Física, Universitat Politècnica de Catalunya (UPC), Barcelona, Spain*
[b]*Departament d'Enginyeria Electrònica, Elèctrica i Automàtica, Universitat Rovira i Virgili (URV), Tarragona, Spain*

Abstract

Cascaded DC-DC converters with source and load converters as their first and last stages are used in wide-ranging applications. Under certain conditions the load converter behaves as a constant power load (CPL) for the source converter. Due to the negative incremental resistance characteristic of the CPL, the system shows instability. One way to overcome this problem is the addition of a loss free resistor (LFR) in series with the inductor of the source converter that stabilizes the system without the loss of global efficiency. The dynamical analysis of fixed duty ratio (open loop) DC-DC boost converter with such a stabilizing resistor and a CPL is studied in this paper by means of an averaged model. Fold and Hopf bifurcations associated to existence and stability of equilibrium are found and the region covered by the basin of attraction of the stable equilibrium is examined. Criteria for choosing the system parameters are exposed accounting for steady state stability and transient conditions. The analysis is performed first for a bidirectional boost converter admitting only continuous conduction mode (CCM) operation and then extended to a unidirectional boost converter where both CCM discontinuous conduction mode (DCM) can take place.

Keywords: DC-DC Converter, Constant Power Load, Loss Free Resistor, Nonlinear Dynamics, Bifurcation.

1. Introduction

DC Distributed Power Systems (DPSs) are now widely used in telecommunication and data centers [1], microgrids [2, 3], electric vehicles (auxiliary power supply as well as motor drive system) [4], space stations, aircraft, ships [5] and many more applications [6] due to the extensive deployment of renewable energy sources and loads of different nature. DPSs have flexible configurations such as cascade, parallel or combination of both [7]. Among them, the use of two-stage cascaded structure of power converters is common in which the first stage is the feeder converter and the second stage is the load converter. The controllers of each source or load converter are designed to regulate either a voltage, a current, or a power reference as per the applications and requirements. Among them, CPL has destabilizing effect on the system [8].

One major stability and performance problem of this configuration is the interaction between the source and load converters even if both the converters are stable and have good dynamical performance individually. Under tight regulation of the output voltage, the load converter behaves as CPL at the output of the source converter. This can be modelled as negative incremental resistance which has destabilizing effect unlike the case of constant voltage load (CVL) or constant current load (CCL). Similar behavior can be observed in DC-AC inverter feeding motor drives [8]. For one-to-one characteristic of speed and torque of the motor and tightly regulated speed, the output power becomes constant (i.e., for every speed, there is one and only one torque) and the motor exhibits CPL behavior to DC-AC inverter.

Switching converters, particularly those fed with CPL, present a fascinating area of study in power electronics due to their unique operational dynamics and implications for system stability and dynamic performance [9, 10]. A CPL is defined as a load that draws a constant amount of power regardless of the input voltage

Email addresses: luis.benadero@upc.edu (L. Benadero), abdelali.elaroudi@urv.cat (A. El Aroudi), max.sebastia@urv.cat (M. Sebastiá-Rullo), kuntal.mandal@urv.cat (K. Mandal), hugo.valderrama@urv.cat (H. Valderrama-Blavi), angel.cid@urv.cat (A. Cid-Pastor), luis.martinez@urv.cat (L. Martínez-Salamero)

or current, which poses specific challenges for the converter's regulation and control. In open loop, switching converters with resistive load exhibits stable dynamics. With resistive load, these converters may be unstable in closed loop designed to maintain the desired output voltage or current. Note that the instability in open loop operation of switching converters is due to the negative incremental resistance characteristics of the CPL and not for any other nonlinearity of the circuit. This phenomenon can result in oscillations or even collapse of the system if not properly managed.

Control strategies become paramount in addressing these challenges; advanced techniques like sliding mode control [11, 12], peak current mode control [13], virtual impedance based control [14], nonlinear control [3, 15] or adaptive control methods [16] can help in mitigating the instability and ensuring robust performance. Additionally, employing feedback mechanisms that account for load variations and implement a compensator can stabilize the dynamics of the converter. Instead of using feedback, to make stable a DC-DC converter with CPL in open loop operation, damping filters can be used [17]. Another way to stabilize these systems is by aggregating parasitic resistances to some key elements such as inductors and switching elements such as transistors and diodes [18]. Because this strategy would imply a reduction in the efficiency of the converter, a convenient alternative solution would be the use of a loss free resistor (LFR). Namely, an LFR is a two-port element with resistive behavior at its input port and transfers the absorbed power at the input port to its output port without losses. This LFR can be synthesized using some switching power converters by imposing the proportionality between the voltage and current at their input port [12].

The interaction between the converter's switching behavior and the CPL needs careful analysis, often requiring the use of simulation tools and experimental setups to explore the dynamic response under different operating conditions. Understanding these interactions is crucial for the design of reliable power supplies in applications ranging from telecommunications to electric vehicles, where maintaining a stable output despite disturbances is critical. Moreover, the dynamics of switching converters under CPL conditions can reveal insights into energy efficiency, electromagnetic interference (EMI), and thermal performance, as the switching frequency and control algorithms impact these factors significantly.

An extensive analysis have been published for the converters feeding CPLs and operating in CCM, but only a few of these converters operating in DCM have been addressed. The stability analysis results were based on averaged models, leading to inaccuracies in predicting the onset of instability in these systems in the parameter space. In [19], it was claimed that the open-loop buck and boost converters operating in DCM are stable when they are loaded by CPLs. Using a nonlinear implicit discrete-time model [20–22], it was shown that such claims about the stability of the buck and the boost converter are not accurate. It is well known that closed-loop switching converters with both resistive loads and CPLs are prone to exhibit a large variety of complex dynamics and undesired instabilities [23, 24].

In all the past research works, a standalone closed-loop converter (buck, boost, resonant etc.) either under voltage mode control (VMC) [25] or current mode control (CMC) [26, 27] were analyzed with a linear load, either resistive [28] or constant current [29] load. The piecewise linear state equations are employed for DC-DC converters to obtain the discrete-time model, and the stability analysis passes through solving the eigenvalues problem of the Jacobian matrix of this model, which can be obtained in closed-form. This is not directly applicable to DC-DC converters loaded by a CPL [13, 30]. The ad hoc stability analysis techniques has been applied. For instance, the piecewise linear approach can still be employed to obtain their approximate discrete-time model and to perform the stability analysis of their periodic orbits, but after a careful linearization of the nonlinear model of the CPL [13]. Recently, an automated stability analysis method is developed for accurate modeling of CPL considering piecewise nonlinear state equations and stability curves are calculated in the parameter space [31].

Overall, the study of switching converters fed by CPL is an evolving field, intertwining theoretical analysis with practical implementations, necessitating a multidisciplinary approach that includes control theory, circuit design, and system engineering. By improving our understanding of these dynamics, we can enhance the design of more efficient, stable, and reliable power electronic systems that cater to the growing demand for advanced power management solutions across various industries. It is interesting to note that open-loop or fixed-ratio switching converters deliver bidirectionality, efficiency and reliability while saving cost, weight in many emerging applications particularly electric vehicle [32] and data centers [33, 34]. The ongoing research and development in this domain highlight the importance of adaptive control techniques and innovative circuit topologies that can dynamically respond to the inherent challenges posed by CPL, paving the way for future advancements in power electronics and energy management systems.

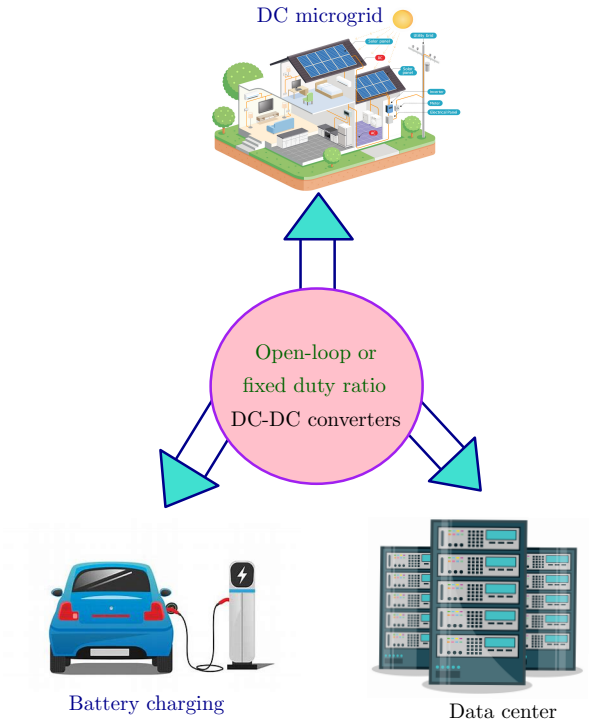

Figure 1: Application of fixed ratio DC-DC converters.

With an extension of earlier works [35, 36], this work deals with the analysis of the dynamics of an open loop DC-DC boost converter with a stabilizing resistor in series with the inductor and a CPL. To simplify the analysis and to provide algebraic explicit mathematical results, an averaged model of the circuit is used with a reduced three dimensional parameter space. This model has two possible equilibrium points, a node and a saddle, whose existence and stability are linked to codimension-one fold and Hopf smooth bifurcations, both emerging from a codimension-two Bogdanov-Takens bifurcation. Actually, the node equilibrium, which can be a focus or not, is the approximation of the desired limit cycle of the real switched system. Then, we get parameter constraint for a correct operation from this analysis. Moreover, an appropriate design requires not only a stable limit cycle with small amplitude, but also that its basin of attraction being wide enough to include normal initial conditions. Then, we make an extended analysis taking into account the global dynamics of the system, mainly related to the saddle stable manifold or to an unstable limit cycle (ULC) whenever it exists. The boundaries for existence in the parameter space of this unstable large amplitude cycle are those corresponding to Hopf bifurcation and a global homoclinic bifurcation, which also emerges from the Bogdanov-Takens bifurcation.

First, in Section 2 an averaged model of the boost converter with a CPL, by using normalized variables and parameters is introduced. Under CCM operation of the system, different limit sets and related bifurcations are demonstrated and also illustrated by means of convenient examples in Section 3. Next in Section 4, operation in DCM is explored with emphasis in its differences with CCM. In both operation modes, the accessibility of the periodic orbit under reasonable initial state conditions is extensively studied. Finally, in the last section the main results are summarized.

2. Circuit: diagram, expressions and normalization

A schematic circuit diagram of the open-loop boost converter feeding a CPL is shown in Fig. 2. The physical parameters V_i, L, C and P represent input voltage source, inductance, capacitance and CPL respectively. R_S is the equivalent virtual resistor for the compensating circuitry [37]. The current through inductor (i_L) and voltage across capacitor (v_C) are taken as state variables of the system. By considering τ as physical time and u as control signal of the switch S, the following differential equations are obtained by applying standard circuit laws in Fig. 2.

$$\begin{aligned} C\frac{dv_C}{d\tau} &= -\frac{P}{v_C} + (1-u)i_L \\ L\frac{di_L}{d\tau} &= -(1-u)v_C - R_S i_L + V_i \end{aligned} \tag{1}$$

The two switches S and $\overline{\text{S}}$ are activated in a complementary way, that is $\overline{u} = 1 - u$. Then if $u = 1$, S is ON (closed) and $\overline{\text{S}}$ is OFF (open). The opposite action is done when $u = 0$. Considering the synchronizing control signals applied to the switches, T_S and d are its period and duty ratio (fraction for which $u = 1$), respectively. From this set of variables and parameters, the following normalized values are defined,

$$t = \omega_0 \tau, \quad x = \frac{v_C}{V_i}, \quad y = \frac{i_L Z_0}{V_i}, \tag{2}$$

where t, x, y are the normalized time and state variables and

$$\omega_0 = \sqrt{\frac{1}{LC}}, \quad Z_0 = \sqrt{\frac{L}{C}}.$$

Besides, normalized parameters CPL (p), complementary duty ratio (q), equivalent resistance (r) and period (T) are

$$p = \frac{PZ_0}{V_i^2}, \quad q = 1 - d, \quad r = \frac{R_S}{Z_0}, \quad T = \omega_0 T_S. \tag{3}$$

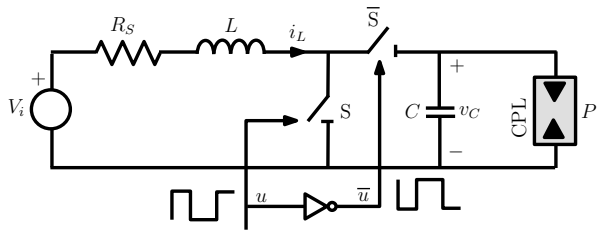

Figure 2: Schematic circuit diagram of a bidirectional open-loop DC-DC boost converter feeding CPL.

Finally, the averaged vector field, that is the normalized differential averaged equations for the state variables (x, y) with parameters p, q, r are summarized as

$$\frac{d\mathbf{x}}{dt} = \dot{\mathbf{x}} = \mathbf{F}(\mathbf{x}) \text{ with } \left\{ \begin{array}{ll} F_x = \dot{x} = & -\frac{p}{x} + qy \\ F_y = \dot{y} = & -qx - ry + 1 \end{array} \right\} \quad (4)$$

where $\mathbf{x} = (x, y)^\intercal$ is the normalized state vector. Notice that binary variable u in the switched model has been substituted by the duty ratio parameter d, and so $(1 - u)$ is replaced by the complementary duty ratio $q = 1 - d$, which is valid in the open interval $(0, 1)$.

In the averaged approach, a continuous time and field are assumed for the evolution of the system, such that the state variables are in fact its averaged values within a cycle, thus replacing the exact switched model by the averaged simplified one. Note that the small amplitude switched limit cycles become equilibrium points in the averaging frame. In Fig. 3, several limit cycles are represented in the state space with different values of the parameters. Note that cycles grow as T increases around the corresponding averaged value represented by a red point. It must be also emphasized that relevant properties of the periodic orbits such as stability suffer minimal variations regarding the averaged approach analyzed below. Fig. 4 shows an illustrative example including the evolution of the state variables at switching instants with period T, its averaged values and also the exponent (that is $\ln(m)/T$) in which m is the characteristic multiplier) computed per cycle. The red dotted line stands for the averaging model approach in the three diagrams for comparisons.

3. Analysis of the continuous conduction mode (CCM) operation

The CCM operation is first analyzed. This condition is not overtaken if $\overline{S}$ is a diode and the inductor current drops to zero. In the next section the discontinuous conduction mode (DCM) operation will be discussed.

3.1. Equilibrium points and associated bifurcations

Two equilibrium points exist for the averaged system (4), whenever $4pr < 1$, which will be called here $\mathbf{x}_N = (x_N, y_N)^\intercal$ and $\mathbf{x}_S = (x_S, y_S)^\intercal$, with values obtained from $\mathbf{F}(\mathbf{x}) = 0$

$$\mathbf{x}_N = \begin{pmatrix} \frac{1 + \sqrt{1 - 4rp}}{2q} \\ \frac{1 - \sqrt{1 - 4rp}}{2r} \end{pmatrix}, \quad \mathbf{x}_S = \begin{pmatrix} \frac{1 - \sqrt{1 - 4rp}}{2q} \\ \frac{1 + \sqrt{1 - 4rp}}{2r} \end{pmatrix} \quad (5)$$

The corresponding pair of eigenvalues λ_N and λ_S associated to $\mathbf{x}_N$ and $\mathbf{x}_S$ respectively, are obtained from the calculated Jacobian matrix which is the equivalent linear system of (4) around equilibrium (5)

$$\lambda_N = \frac{1}{2}\left(\frac{p}{x_N^2} - r \pm \sqrt{W_N}\right), \text{ where } W_N = \left(\frac{p}{x_N^2} + r\right)^2 - 4q^2 \quad (6)$$

$$\lambda_S = \frac{1}{2}\left(\frac{p}{x_S^2} - \pm \sqrt{W_S}\right), \text{ where } W_S = \left(\frac{p}{x_S^2} + r\right)^2 - 4q^2 \quad (7)$$

Note that under the critical parameter condition $4rp = 1$, both equilibrium collapse at the common fold point $\mathbf{x}_F$ with eigenvalues λ_{F1} and λ_{F2},

$$\mathbf{x}_F = \left(\frac{1}{2q}, \frac{1}{2r}\right)^\intercal, \quad \lambda_{F1} = 0, \quad \lambda_{F2} = \frac{q^2}{r} - r. \quad (8)$$

Remark 1. From these results, we conclude that in system (4), for the critical parameter condition $p = p_F = (4r)^{-1}$, the two equilibrium collapse, being null one of the common eigenvalues thus resulting a smooth fold, also called saddle-node, codimension-one bifurcation.

Note that for this condition, the nonzero eigenvalue meets the condition $\lambda_{F2} > 0$ if $q > r$ or $\lambda_{F2} < 0$ if $q < r$. In the boundary of these two cases, we have $q = r$

Remark 2. In system (4), for the two critical parameter conditions $p = p_F = (4r)^{-1}$ and $q = r$, in addition to the equilibrium extinction, their two common eigenvalues become null, thus resulting a codimension-two Bogdanov-Taken bifurcation.

Remark 3. Moreover, for the critical parameter point as $\mathcal{P}_1 \equiv \{r = 1, p = 1/4, q = 1\}$, such that the codimension-two Bogdanov-Taken bifurcation is located at one extreme value ($d = 0$) of the duty ratio domain. Then, if $r > 1$, Hopf bifurcation cannot take place since this bifurcation only exists if $r < 1$, thus starting at codimension-two Bogdanov-Takens, according to Remark 2 .

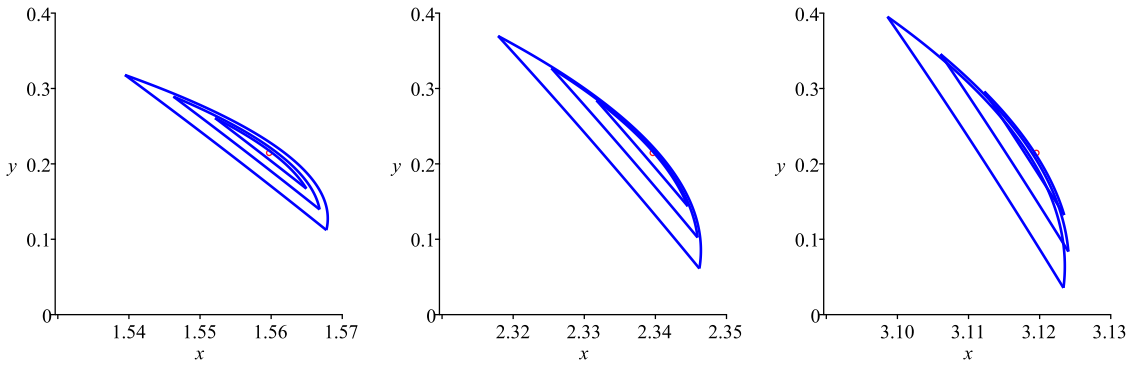

(a) $q = 0.6$ ($d = 0.4$) (b) $q = 0.4$ ($d = 0.6$) (c) $q = 0.3$ ($d = 0.7$)

Figure 3: Limit cycles (periodic orbits) with parameters $r = 0.3, p = 0.2, T \in \{0.25, 0.40, 0.55\}$ and q in the caption. Red points correspond to equilibrium in the averaging approach.

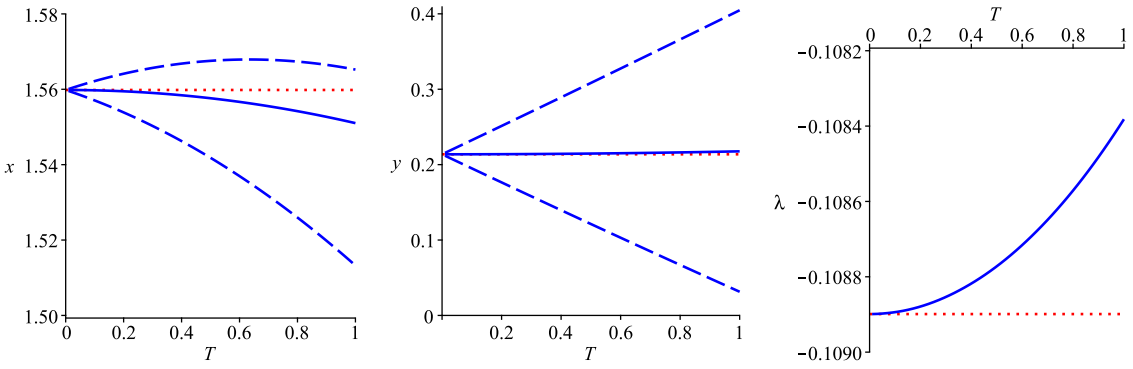

(a) $x(T)$ (b) $y(T)$ (c) $\lambda(T)$

Figure 4: (a-b) state variables at the switching instants (blue dashed lines) and computed averaged values per cycle (blue line). (c) numerically computed exponent. The red dotted line stands for the averaging model approach in the three diagrams for comparisons. Parameters are $r = 0.3, p = 0.2, q = 0.6$ ($d = 0.4$) and varying T is in the abscissa.

In order to check the evolution of the eigenvalues λ_N and λ_S for the two equilibrium $\mathbf{x}_N$ and $\mathbf{x}_S$, with parameters $r > 0, 0 < p < p_F = (4r)^{-1}$ and $q \in (0, 1)$, we evaluate W_N and W_S in (6) and (7) respectively, taking into account x_N and x_S in (5). Noticing that either W_N or W_S are expressed as a square difference of two terms, both of them positive, therefore the radicand can only permute its sign when the difference of the two terms, called here Σ_N or Σ_S vanishes. These magnitudes are

$$\Sigma_N = \frac{q^2}{\sigma_N} + r - 2q, \text{ where } \sigma_N = \frac{1 - 2rp + \sqrt{1 - 4rp}}{2p} \tag{9}$$

$$\Sigma_S = \frac{q^2}{\sigma_S} + r - 2q, \text{ where } \sigma_S = \frac{1 - 2rp - \sqrt{1 - 4rp}}{2p} \tag{10}$$

We check that $\Sigma_S > 0$ in our parameter domain, so $\mathbf{x}_S$ is always a saddle.

However, concerning $\mathbf{x}_N$, $\Sigma_N = 0$ if $q = q_W = \sigma_N\left(1 \pm \sqrt{1 - r/\sigma_N}\right)$. Besides, $\Sigma_N = 0$ if $q = r/2$ with $p = 0$ and also, $\Sigma_N = 0$ if $d = 0$ with $p = p_0 = (2 - r)(1 + 2r - r^2)^{-2}$. Therefore, if $r < 1$, the positive branch is valid in the range $q_W \in (r, 1)$ corresponding to p from p_0 to p_F and the negative branch is valid in the range $q_W \in (r/2, r)$ corresponding to p from p_F to 0. If $1 < r < 2$, the positive branch for q_W is not valid and the negative one is given for $q_W \in (r/2, 1)$ associated to p from p_0 to 0. If $r > 2$, no branch applies for q_W, so the node is always non spiral and stable.

Crossing the positive q_W branch implies a transition for the equilibrium node $\mathbf{x}_N$ between spiral or focus and non spiral behavior. The positive branch stands for unstable node and the negative one for the stable node.

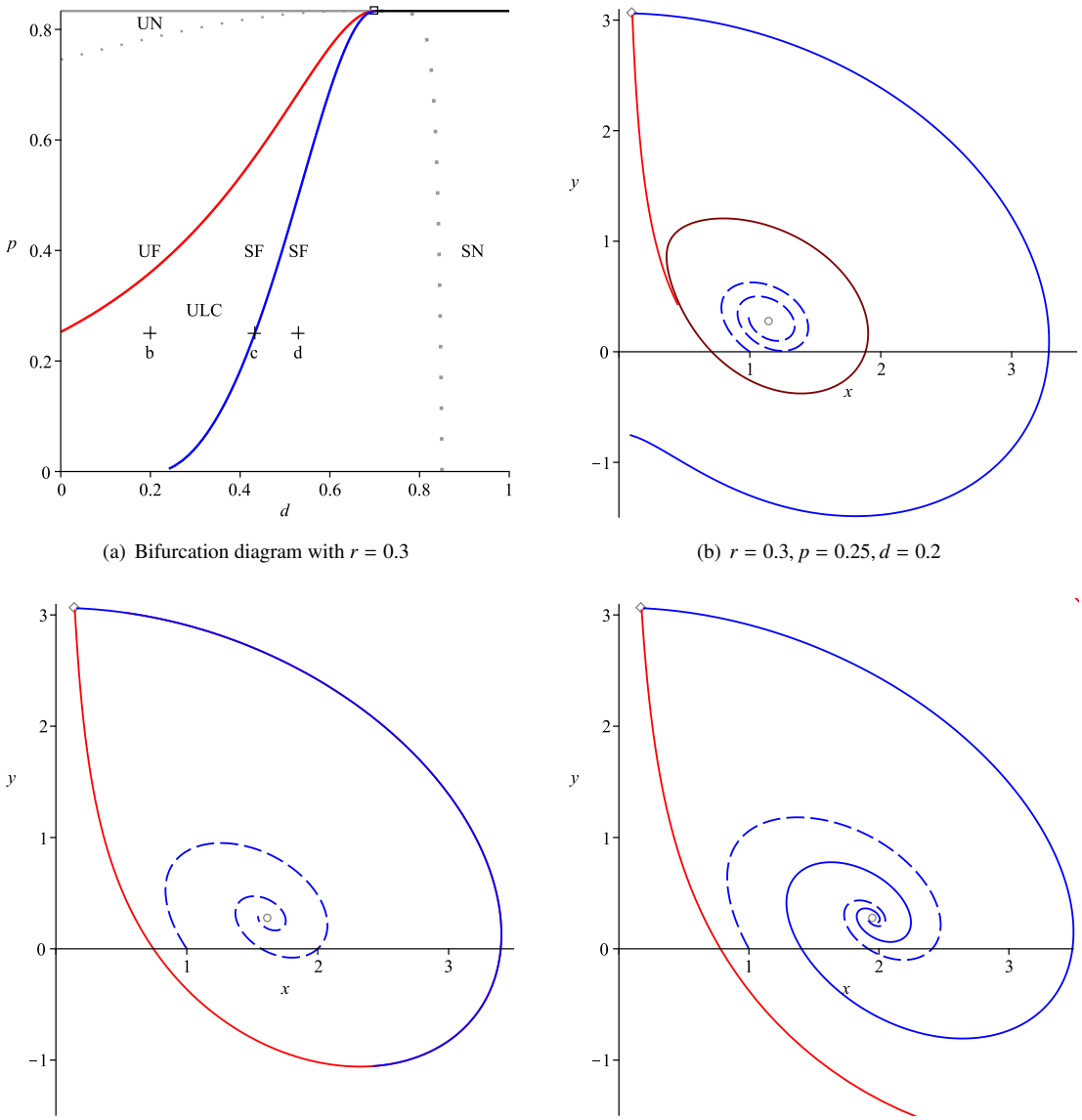

(a) Bifurcation diagram with $r = 0.3$

(b) $r = 0.3, p = 0.25, d = 0.2$

(c) $r = 0.3, p = 0.25, d = 0.432796$

(d) $r = 0.3, p = 0.25, d = 0.53$

Figure 5: (a) Diagram in $d - p$ parameter plane using $r = 0.3$, including bifurcation lines: fold (black), Hopf (red), homoclinic (blue), and also the spiral to non spiral transition (dotted line). The possible equilibrium, SF or UF and SN or UN (stable or unstable focus and stable or unstable node) are indicated in their existence regions. Besides, the ULC (unstable limit cycle) exists in the parameter region between Hopf and homoclinic bifurcations. Notice also that the saddle equilibrium exists for $p < (4r)^{-1}$ and the codimension-two bifurcation is given at $p = (4r)^{-1}, q = r$ (boxed point), from which the one dimensional bifurcating lines emerge. (b-d) Dynamics in the state plane with parameters in the caption (cross points in panel (a) stand for these values), including relevant invariant sets: the stable spiral node and the saddle equilibrium (circle and diamond points), the stable and unstable saddle manifolds (red and blue lines), and the orbit from $(1, 0)$ state (dashed blue line). Case (b) includes also the ULC (closed line) and case (c) approaches the homoclinic bifurcation for which the stable and unstable saddle manifolds merge together.

The next and relevant question concerns stability. The spiral node $\mathbf{x}_N$, with an associated frequency $\sqrt{-W_N}$, becomes unstable when the real part of λ_N vanishes, which occurs at the critical value

$$q_H = 1 - \sqrt{r\sigma_N}, \tag{11}$$

where σ_N is defined in (9). Actually, this is a smooth subcritical Hopf bifurcation, at which an unstable limit cycle (ULC) is born. More details about the existence and significance of this limit cycle, which coexists with the stable spiral equilibrium $\mathbf{x}_N$, will be given below.

In Fig. 5, the continuous black and red lines stands for the smooth fold (emergence of the saddle and stable node pairs) and the subcritical Hopf (stability boundary of the spiral node) bifurcations respectively. The continuous gray line is associated to the saddle and unstable node pair appearance. The sparse dots line corresponds to the transition between spiral and non spiral behavior of the node.

The following subsections deal with the feasibility of reaching the stable equilibrium whenever it exists, thus concerning the boundary of its attraction basin. We will concentrate on two conditions. As a stricter one, the inclusion in that basin of the state $(1, 0)$, as a likely starting point of the dynamics, is considered. As a second more relaxed condition, we impose that at least one point of the abscissa, that is $\mathbf{x} = (x, 0)$, belongs to the basin. In order to find critical parameter values for which these conditions apply, two excluding cases are possible. One refers to the ULC, and the stable saddle manifold (SSM) is involved in the second case. As it is well known these two invariant sets can be boundaries of an attraction basin. If the ULC exists, this set will determine the critical condition, otherwise the SSM will do. Thus, the existence of the ULC will be examined first.

3.2. Homoclinic bifurcation and existence of the unstable limit cycle

In order to delimit the parameter subset for which the unstable limit cycle (ULC) exists, we must pay attention to the homoclinic bifurcation emerging from the smooth Bogdanov-Takens bifurcation of the equilibrium examined above. This is a global bifurcation, for which the stable saddle manifold (SSM) is superimposed to the unstable saddle manifold (USM) of the same saddle equilibrium point (the heteroclinic bifurcation stands for a similar interaction involving two saddle points). From a numerical continuation procedure implemented on Maple© platform, we have determined the set of points for this bifurcation, fixing one parameter and solving for the other. In Fig. 5(a), made using fixed parameter $r = 0.3$, the continuous blue line stands for the homoclinic bifurcation set in the $(d - p)$ parameter plane. Figure 5(c) is a state diagram with a parameter selection near the homoclinic bifurcation. Note that in the parameter region between the Hopf (red) and homoclinic (blue) lines, the node is an spiral equilibrium, and the unstable saddle manifold cannot end at that point as it avoids crossing the SSM (stable saddle manifold). Thus forces the existence of an extra invariant set in the form of an unstable limit cycle splitting the state space in two regions. Orbits starting inside the ULC flow to the SF (stable focus) equilibrium, see Figure 5(b). Conversely, with parameters such in Figure 5(d), the SSM itself is the separatrix of the desired orbits flowing to the SF or the undesired ones collapsing as approaching to $x = 0$.

Taking into account that the codimension-two Bogdanov-Takens exists only for parameter $r < 1$, with values $p = (4r)^{-1}, q = r$, the homoclinic bifurcation can only be given with the same restriction $r < 1$. In such a case the attracting basin of the stable focus is an unstable limit cycle in the parameter region between the Hopf and the homoclinic lines. Outside this parameter region if $r < 1$, or in any case if $r > 1$, the stable saddle manifold defines the attraction basis of the stable (spiral or not) node, whenever it exists. In the following section, we will determine the parameter regions for which orbits starting at the state $(1, 0)$ flows to the stable equilibrium.

A critical parameter set, dealing with the structure of parameters defining an attracting domain passing through the critical state $(1, 0)$, is obtained numerically by imposing the following three restrictions: homoclinic bifurcation tangent to $(1, 0)$ at the value $d = 0$. Approximately, this is $\mathcal{P}_2 \equiv \{r \simeq 0.695540, p \simeq 0.262139, q = 1\}$.

3.3. Parameter set associated to state $(1, 0)$ in the boundary of the attracting basin of the stable equilibrium

In order to determine the frontier in the parameter space, for which orbits with initial state $(1, 0)$ either flows or not to the equilibrium, one of the two possible scenario examined above must be selected according to the given criteria. If $r < 0.695540$ (thus value corresponds to r at $\mathcal{P}_2$) and inside the parameter area between the Hopf and the homoclinic bifurcation lines, the frontier line should be determined forcing the unstable limit cycle passing through $(1, 0)$. $p(d)$ parameter relation with r fixed is given in Fig. 6 using green long dashed lines. Otherwise, the frontier line, if exists, is determined forcing the SSM passing through $(1, 0)$. Green dot-dash lines, also in Fig. 6, correspond to this second case.

As a second more relaxed condition, we impose that at least one point of the abscissa, that is $\mathbf{x} = (x, 0)$ belongs to the basin; actually, this point is tangent to the abscissa. If this condition were not satisfied, dynamics will not flow to equilibrium with a starting null inductor current condition with any value of the initial capacitor voltage. As in the above cases for boundary at $(1, 0)$, this condition should be applied either to the ULC or to the SSM. Orange lines in Fig. 6 stand for these more

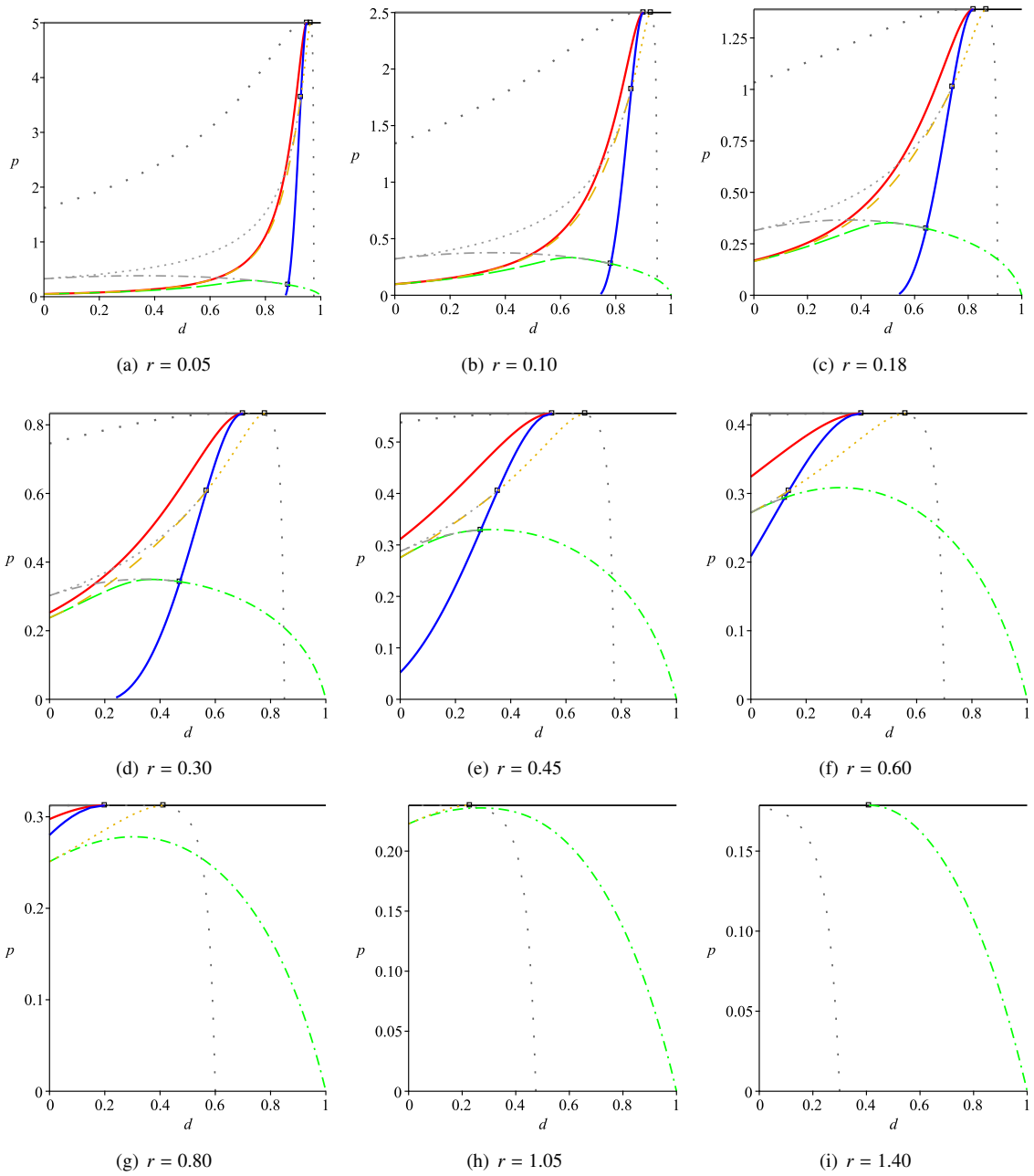

(a) $r = 0.05$ (b) $r = 0.10$ (c) $r = 0.18$

(d) $r = 0.30$ (e) $r = 0.45$ (f) $r = 0.60$

(g) $r = 0.80$ (h) $r = 1.05$ (i) $r = 1.40$

Figure 6: Stable saddle manifold (SSM) and unstable saddle manifold (USM) in $d - p$ parameter plane for different values of r.

relaxed cases, dashed are for ULC and dot-dashed for SSM.

In order to give a more complete view, some alternative representations are given in Fig. 7. In panels (a-c) of this figure, the critical $p(r)$ condition for the boundary at $(1, 0)$, if exists, is plotted for fixed values of parameter d in the caption. Long dash green lines stand for ULC case, green dot dash lines apply to SSM case and black lines do for the fold existence limit. In this last case, $(1, 0)$ belongs always to the basin of equilibrium. The connection between those cases is represented by boxed points. In panel (d), a set of lines in the $d - p$ parameter plane are plotted with several fixed values of parameter r. From these diagrams, we can appreciate that certain parameter combinations are more suitable in order to optimize the attraction basin of equilibrium,

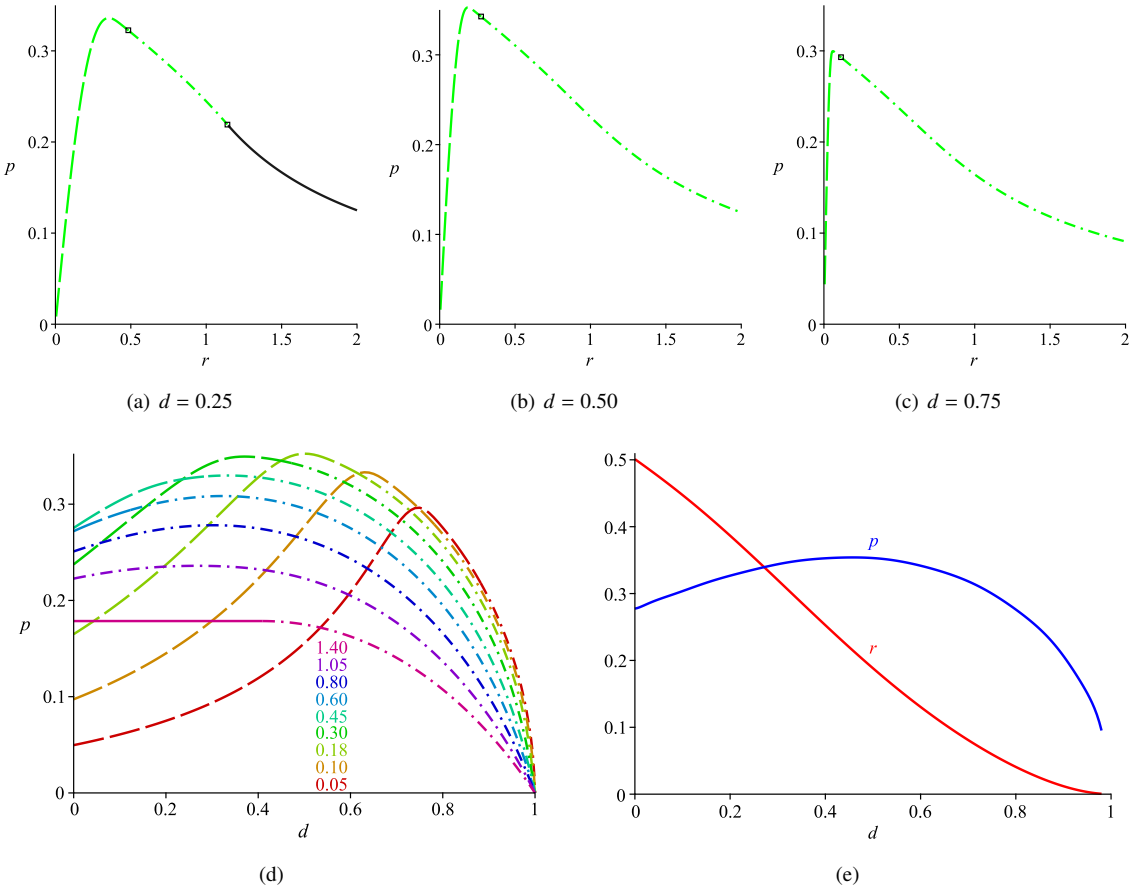

(a) $d = 0.25$ (b) $d = 0.50$ (c) $d = 0.75$

(d) (e)

Figure 7: Diagrams related to basin attraction boundary at $(1, 0)$: (a-c) $r(p)$ with d in the caption, (d) $p(d)$ with legend for r inside the panel and (e) r, $p(d)$ values that optimize this boundary.

thus avoiding undesired dynamics if $(1, 0)$ is assumed as the starting state. In the panel (e), we represent the optimal value of r (red line) in front of the duty ratio d, thus providing a maximum available value of p with safe conditions, which is also shown in the same diagram (blue line). Note that this situation always corresponds to the ULC as the attraction basin including the state $(1, 0)$.

4. Limit cycles in discontinuous conduction mode

Up to now, it is assumed that the circuit is bidirectional and the current can flow in both directions so that only CCM is possible, due to the use of bidirectional switches or instead, the inductor current remains always positive. From now, the complementary switch ($\overline{S}$) is assumed to be a diode (see Fig. 9), so that the inductor current cannot be negative. The standard periodic orbit in the DCM operation has three time intervals. The first two correspond to ON and OFF equations (4). The third interval starts when $y(t)$ drops to zero in the OFF condition and finish at the beginning of a new clock period, thus re-initiating the ON state. In this third interval, apart from condition $y = 0$, we have the differential equation

$$\dot{x} = -\frac{p}{x}. \tag{12}$$

In Fig. 8, parameters r and d have been fixed. In the panel (a) of this figure, T is also fixed and p is decreased so as to reach the CCM-DCM boundary at the critical value p_C. Besides, in the panel (b), p is fixed and T is increased until the critical T_C (see numerical values in the panel captions). If those parameters are further varied, then limit cycle enters DCM operation, as it can be shown in panels (c-d) of the same figure. The onset of DCM operation is also given if d is increased or if r is decreased, while the other parameters are constant.

In [38], DCM periodic orbits are extensively analyzed, showing a complexity outbreak when the nor-

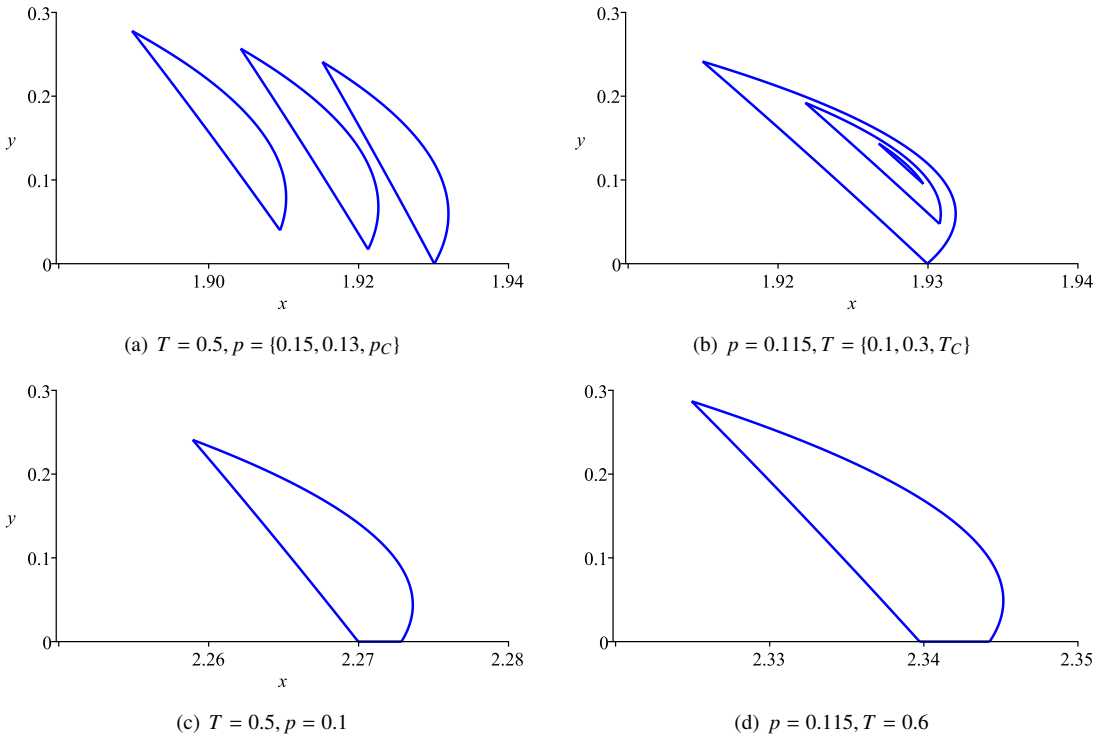

(a) $T = 0.5, p = \{0.15, 0.13, p_C\}$

(b) $p = 0.115, T = \{0.1, 0.3, T_C\}$

(c) $T = 0.5, p = 0.1$

(d) $p = 0.115, T = 0.6$

Figure 8: Limit cycles with parameters $r = 0.3, d = 0.5$ and p, T in the caption. Note that DCM is attained in (a), by decreasing p, at critical $p_C \simeq 0.114767$, and in (b), by increasing T, at $T_C \simeq 0.501105$. Further variation of the same parameter makes the dynamics entering in DCM operation as it can be seen (c-d).

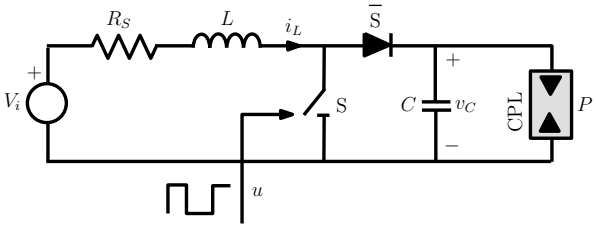

Figure 9: Schematic circuit diagram of a unidirectional open-loop DC-DC boost converter feeding CPL where the complementary switch ($\overline{S}$) is replaced by a diode.

malized period T is increased. In the current work, we are dealing only with low or moderate values of T, so that only main existence boundaries are relevant and the DCM limit cycle remains stable. Let us summarize here an averaged model that fairly approaches the dynamics in DCM. In the following, d' is the duty ratio during the OFF interval until y becomes null. Then $1-d-d'$ is the ratio corresponding to condition $y = 0$.

Let first assume that during d and d' ratios, the average value y_1 of $y(t)$ is approximately equal to half of the peak value for $y(t)$. Then from $2y_1 = (1 - ry_1)dT$ and $(1 - ry_1)d = (x + ry_1 - 1)d'$, we have

$$y_1 = \frac{dT}{2 + rdT}, \qquad d' = \frac{2d}{(2 + rdT)x - 2.} \tag{13}$$

From y_1 and d', by considering very small variations in $x(t)$ and taking into account that $y = 0$ during the third time interval, from $y_S(x) = y_1(d + d')$ the explicit which links state variables y and x follows

$$y_S = \frac{d^2 T x}{(2 + rdT)x - 2} \tag{14}$$

Note that (14) is only valid under $d+d' < 1$ condition, so the dynamics sliding on $y_S(x)$ has a natural limit $\mathbf{x}_B = (x_B, y_B)$ such that if $x < x_B$ (equivalently $y > y_B$), the CCM mode is restored.

$$x_B = \frac{2}{q(2 + rdT)}, \qquad y_B = \frac{dT}{2 + rdT}. \tag{15}$$

Note also that using the averaging approach, the dynamical model is reduced in one dimension so the dynamics is constrained along the line $y_S(x)$ whose vector field velocity is given by $-p/x + y_1 d'$, thus resulting

$$\frac{dx}{dt} = -\frac{p}{x} + \frac{2d^2 T}{((2 + rdT)x - 2)(2 + rdT)}. \tag{16}$$

Also, by equaling to zero the field in (16), that is the average equilibrium condition, an approach to the location of the DCM limit cycle is obtained. This point called here $\mathbf{x}_D = (x_D, y_D)$ has as coordinates

$$x_D = \frac{2(2+rdT)p}{(2+rdT)^2 p - 2d^2 T}, \quad y_D = \frac{(2+rdT)p}{2}. \quad (17)$$

Regarding the hyper-surface in the parameter space splitting DCM and CCM operation, it can be easily deduced from equaling $y_D = y_B$ (this is equivalent to force $d + d' = 1$ in equilibrium), thus giving to an explicit expression for the critical value p_C, such that if $p > p_C$, the periodic orbit enters in CCM.

$$p_C = \frac{2dT}{(2+rdT)^2}. \quad (18)$$

Furthermore, the DCM solution needs an extra condition, which is straightforward by imposing a positive value for x_D, so a natural limit condition is obtained making null the denominator of x_D in (17). If this critical parameter is called p_I, the existence condition for the DCM limit cycle is $p_I < p < p_C$, being

$$p_I = \frac{2d^2 T}{(2+rdT)^2}. \quad (19)$$

The existence condition $p_I < p < p_C$, can be expressed in terms of the dimensionless parameter K as $K_I < K < K_C$, in which K, K_C, K_I are

$$K = \frac{2p}{T} = \frac{2LP}{TV_i^2}, K_I = \left(\frac{2d}{2+rdT}\right)^2, K_C = \frac{4d}{(2+rdT)^2} \quad (20)$$

Notice that if $r = 0$, the existence condition is simplified as $d^2 < K < d$ (see [38]). It is also of interest the fact that all the above expressions contain the term $rdT = (dT_S)/(L/R_S)$, which is the relation between the time interval in the ON configuration and the time constant associated to the resistor in series with the inductor. As far as this value is small compared with 2, the features of the DCM limit cycle approaches more the behavior analyzed in [38].

In Fig. 10, using parameters r, T fixed, the two boundaries concerning the existence of DCM cycles in the parameter plane (d, p) is depicted in panel (a). The same limits are also plotted in (b), but in the plane (d, K). Corresponding black solid lines stand for (18) and (19) in (a) and for (20) in (b). Cross points over these lines have been obtained by numerical computation; notice there is a good agreement between them and the algebraic expressions. Summarizing, concerning the limit cycle in CCM apart from existence and stability conditions analyzed in Section 3, its existence is also limited by condition in (18). Above or below this line, CCM or DCM is given respectively. Also DCM cannot exist below line for condition in (18). However, there are some extra lines in 10(b), due to partial DCM operation, which concerns mainly the attractor basin of the periodic orbit. The unstable large limit cycle and also a stable large limit cycle (long period and large amplitude both) encircling the former unstable one are responsible of the new features.

4.1. Large stable and unstable cycles operated in DCM

Initially, after emerging at the Hopf bifurcation, the large unstable limit cycle (ULC) operates in CCM, so no difference exists with above analysis. However, it is extinguished when colliding with the sliding line in the phase plane, see (14). Actually, this is a nonsmooth fold bifurcation, from which a large stable limit cycle (SLC) also emerges, both coexisting in some range of parameters. In Fig. 11, made with fixed parameters $r = 0.3, d = 0.35, T = 0.3$ and p variable, the amplitude of these large cycles is shown. Note on the right the Hopf bifurcation at critical $p_H \simeq 0.482570$, On the right ($p > p_H$), the (averaged) equilibrium becomes unstable (dotted red line). On the left ($p < p_H$), the stable equilibrium (solid green line) coexists with the unstable large limit cycle, which acts as basin boundary of equilibrium. Finally, on the left of the diagram, from the nonsmooth fold bifurcation at $p_F \simeq 0.43129$, the two stable (solid green line) and unstable large limit cycles emerge, thus existing in some range for $p > p_F$. Violet lines in Fig. 10(b) concern also to the existence of the two stable and unstable large limit cycles. More precisely, the ULC exists between the solid red line (Hopf) and the solid violet line (nonsmooth fold), and the SLC exists between this last line and the dashed violet line. This last limit is due to approaching the SLC to $x = 0$ (then dynamics makes nonsense). In the same panel, cross points superimposed to the Hopf line (solid red) account for exact computations. Actually, this is a Neimark-Sacker bifurcation (the discrete counterpart of the Hopf with the exact switched model). Notice that the averaged model has good degree of precision and is very easy to use compared to the exact switched model.

To complete the description of Fig. 10(b), the dot-dashed green line splits the parameter plane in regions for which the boundary of equilibrium includes (below) or not (above) the likely starting point $(1, 0)$. This line is not plotted after colliding to the solid violet line (nonsmooth fold case), because the ULC itself avoids the dynamics convergence from $(1, 0)$ to equilibrium because it entirely lies on $y > 0$ half plane. Notice also that

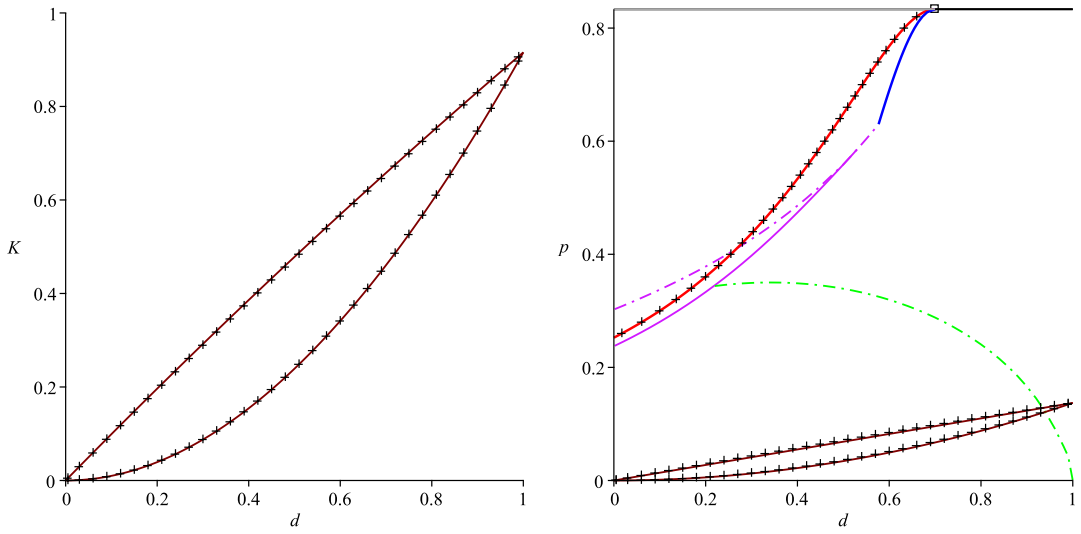

Figure 10: (a) Lines in $K(d)$ plane are existence boundaries for DCM periodic orbit. The upper one limits with CCM and the lower one refers to $x \to \infty$. Cross points have obtained with the exact switched model to verify the validity of the averaging approach. In (b), beside the same limits, the still valid boundaries reported in Fig. 5(d) are plotted in addition to the existence boundaries for the large limit cycles (low frequency oscillations). Fixed parameters in the two diagrams are $r = 0.3$ and $T = 0.3$.

the homoclinic (solid blue) line only makes sense until colliding the sliding line, see (14).

In Fig. 11(b-f), the particular large limit cycles (low frequency oscillations) using parameters $r = 0.3, p = 0.45, d = 0.35, T = 0.3$ are represented, (a) both oscillations in the phase plane, (c-d) are $x(t)$ oscillograms and (e-f) are $y(t)$ representations. The unstable cycle is in (c,e) and the stable one is in (d,f). The switched dynamics and also the average one have been included in these representations. Note the good agreement between them. Regarding the switched dynamics, it can be either quasiperiodic, or periodic in case of phase locking between the switching high frequency oscillation and the low frequency oscillation .

5. Conclusions

The dynamics of an open loop DC-DC boost converter feeding a CPL and a series loss free resistor has been analyzed in continuous and discontinuous conduction mode of operation. The comparison of the results are shown by using averaged and exact switched models. With the variation of the system parameters, the equilibria, saddle manifolds and low frequency large amplitude oscillations are found and their related bifurcations are analyzed. Accessibility of the desired dynamics (equilibrium in the averaging approach) is also considered by examination of the region covered by the basin of attraction of equilibrium. This study can also be extended to other converter topology to showcase similar or new types of bifurcation mechanism leading to complex behaviors.

After knowing the different mechanism of smooth and nonsmooth bifurcations with the variation of the parameters, suitable bifurcation control can be applied to avoid/delay the bifurcation point. Therefore the reliable operation range could be extended in the parameter space. As the open loop or fixed ratio converter fed CPL has many emerging applications in electric vehicle, data centers etc, the accumulated results from this study will be helpful to devise novel control law to extend the stability margin of the overall system.

It is worth noting that the conventional techniques such as the descriptive function (DF) method for predicting the existence of limit cycles and their stability could be used for the system considered in this study. However, encountering a DF that takes into account all the nonlinearities of the system and catches the nonlinear large signal behavior reported in this study is challenging. A DF that only accounts for one nonlinearity and overlooks others may fail short in predicting the global behavior of the system.

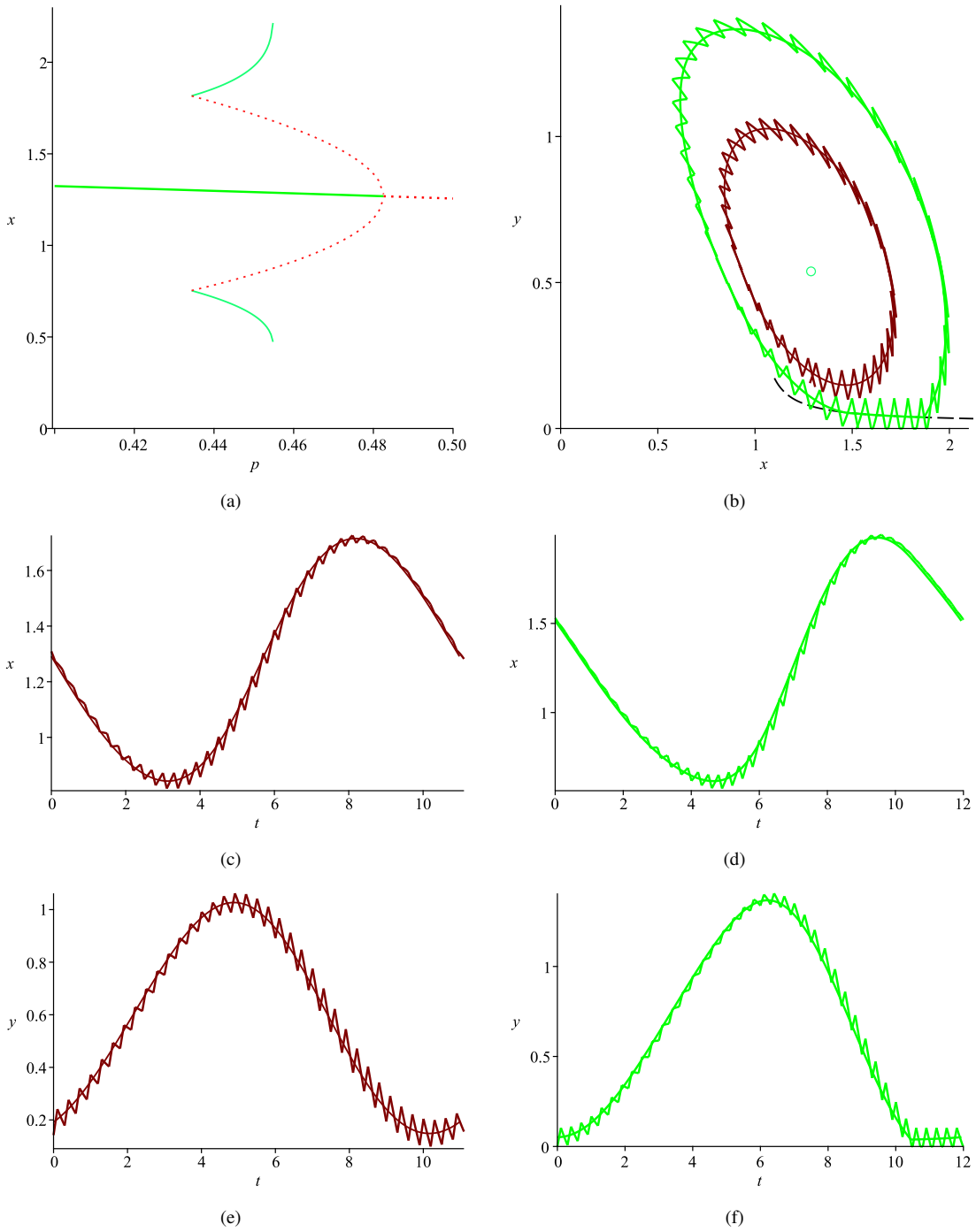

Figure 11: Bifurcation diagram $x(p)$ with $r = 0.3, d = 0.35, T = 0.3$ giving the evolution of equilibrium and amplitude of the low frequency oscillations. Dotted red and solid green lines refers to unstable and stable cases. (a-f) are representations of low frequency oscillations with the above parameters and $p = 0.45$. Diagrams are (a) in the phase plane, $x(t)$ is in (c,d) and $y(t)$ in (d,f). Maroon and green lines refer to unstable and stable cases respectively. The switched dynamics and also the average one have been included in these representations. Note the good agreement between them.

Acknowledgements

This work was sponsored by the Spanish Ministerio de Ciencia e Innovación under Grant PID2023-150839OB-I00. K. Mandal acknowledges support from

the Agency for Management of University and Research Grants (AGAUR) under the Ministry of Research and Universities of the Government of Catalonia (Grant Reference No. 2020 BP 00260).

References

[1] P. T. Krein, Data center challenges and their power electronics, CPSS Transactions on Power Electronics and Applications 2 (1) (2017) 39–46.

[2] T. Dragicevic, X. Lu, J. C. Vasquez, J. M. Guerrero, Dc microgrids - part i: A review of control strategies and stabilization techniques, IEEE Transactions on Power Electronics 31 (7) (2016) 4876–4891.

[3] A. Kwasinski, C. N. Onwuchekwa, Dynamic behavior and stabilization of dc microgrids with instantaneous constant-power loads, IEEE Transactions on Power Electronics 26 (3) (2011) 822–834.

[4] L.-M. Saublet, R. Gavagsaz-Ghoachani, J.-P. Martin, B. Nahid-Mobarakeh, S. Pierfederici, Bifurcation analysis and stabilization of dc power systems for electrified transportation systems, IEEE Transactions on Transportation Electrification 2 (1) (2016) 86–95.

[5] C. H. Rivetta, A. Emadi, G. A. Williamson, R. Jayabalan, B. Fahimi, Analysis and control of a buck dc-dc converter operating with constant power load in sea and undersea vehicles, IEEE Transactions on Industry Applications 42 (2) (2006) 559–572.

[6] M. Z. Hossain, N. A. Rahim, J. a/l Selvaraj, Recent progress and development on power dc-dc converter topology, control, design and applications: a review, Renewable and Sustainable Energy Reviews 81 (1) (2018) 205–230.

[7] Ericsson Power Modules, Selection of Architecture for Systems using Bus Converters and POL Converters, Design Note 023 (July 2010).

[8] A. Emadi, A. Khaligh, C. H. Rivetta, G. A. Williamson, Constant power loads and negative impedance instability in automotive systems: definition, modeling, stability, and control of power electronic converters and motor drives, IEEE Transactions on Vehicular Technology 55 (4) (2006) 1112–1125.

[9] L. Benadero, R. Cristiano, D. J. Pagano, E. Ponce, Nonlinear analysis of interconnected power converters: a case study, IEEE Journal on Emerging and Selected Topics in Circuits and Systems 5 (3) (2015) 326 – 335.

[10] R. Cristiano, D. J. Pagano, L. Benadero, E. Ponce, Bifurcation analysis of a dc-dc bidirectional power converter operating with constant power loads, International Journal of Bifurcation and Chaos 26 (4) (2016) 1630010.

[11] A. Cid-Pastor, L. Martinez-Salamero, A. El Aroudi, R. Giral, J. Calvente, R. Leyva, Synthesis of loss-free resistors based on sliding-mode control and its applications in power processing, Control Engineering Practice 21 (2013) 689–699.

[12] R. Haroun, A. El Aroudi, A. Cid-Pastor, E. Vidal-Idiarte, H. Valderrama-Blavi, L. Martinez-Salamero, Modelling and control of modular dc-nanogrids based on loss-free resistors, IEEE Access 8 (2020) 33305–33317.

[13] A. El Aroudi, M. S. Al-Numay, R. Haroun, , G. Zhang, Analytical determination of fast-scale instability boundaries for current mode controlled dc–dc converters with cpl and closed voltage loop, IEEE Journal on Emerging and Selected Topics in Circuits and Systems 11 (1) (2021) 39–48.

[14] S. Karan, K. Mandal, S. K. Chattopadhyay, Virtual impedance based lyapunov controller for dc-dc converter-fed constant power load, 48th Annual Conference of the IEEE Industrial Electronics Society (2022 IECON), Brussels, Belgium, 2022.

[15] B. A. Martinez-Treviño, A. El Aroudi, A. Cid-Pastor, L. Martinez-Salamero, Nonlinear control for output voltage regulation of a boost converter with a constant power load, IEEE Transactions on Power Electronics 34 (11) (2019) 10381–10385.

[16] X. Zhang, X. Ruan, H. Kim, C. K. Tse, Adaptive active capacitor converter for improving stability of cascaded dc power supply system, IEEE Transactions on Power Electronics 28 (4) (2013) 1807–1816.

[17] R. W. Erickson, D. Maksimovic, Input Filter Design. Fundamentals of Power Electronics, Springer International Publishing, 2020.

[18] A. Khaligh, Realization of parasitics in stability of dc–dc converters loaded by constant power loads in advanced multiconverter automotive systems, IEEE Transactions on Industrial Electronics 55 (6) (2008) 2295–2305.

[19] A. M. Rahimi, A. Emadi, Discontinuous-conduction mode dc/dc converters feeding constant-power loads, IEEE Transactions on Industrial Electronics 57 (4) (2010) 1318–1329.

[20] J. Deane, D. Hamill, Instability, subharmonics, and chaos in power electronic systems, IEEE Transactions on Power Electronics 5 (3) (1990) 260–268.

[21] M. di Bernardo, F. Vasca, Discrete-time maps for the analysis of bifurcations and chaos in dc/dc converters, IEEE Transactions on Circuits and Systems I: Fundamental Theory and Applications 47 (2) (2000) 130–143.

[22] A. El Aroudi, D. Giaouris, H. H.-C. Iu, I. A. Hiskens, A review on stability analysis methods for switching mode power converters, IEEE Journal on Emerging and Selected Topics in Circuits and Systems 5 (3) (2015) 302–315.

[23] S. Banerjee, G. C. Verghese, Nonlinear Phenomena in Power Electronics — Attractors, Bifurcations, Chaos, and Nonlinear Control, New York : IEEE Press, 2001.

[24] C. K. Tse, Complex Behavior of Switching Power Converters, Boca Raton: CRC Press, 2003.

[25] K. Chakrabarty, G. Poddar, S. Banerjee, Bifurcation behavior of the buck converter, IEEE Transactions on Power Electronics 11 (3) (1996) 439–447.

[26] J. Deane, Chaos in a current-mode controlled boost dc-dc converter, IEEE Transactions on Circuits and Systems I: Fundamental Theory and Applications 39 (8) (1992) 680–683.

[27] C. Tse, Chaos in a current-mode controlled boost dc-dc converter, International Journal of Circuit Theory and Applications 22 (4) (1994) 263–278.

[28] E. Fossas, G. Olivar, Study of chaos in the buck converter, IEEE Transactions on Circuits and Systems I: Fundamental Theory and Applications 43 (1) (1996) 13–25.

[29] L. Cheng, W.-H. Ki, F. Yang, P. K. T. Mok, X. Jing, Predicting subharmonic oscillation of voltage-mode switching converters using a circuit-oriented geometrical approach, IEEE Transactions on Circuits and Systems I 64 (3) (2017) 717–730.

[30] A. El Aroudi, R. Haroun, M. Al-Numay, J. Calvente, R. Giral, Fast-scale stability analysis of a dc–dc boost converter with a constant power load, IEEE Journal of Emerging and Selected Topics in Power Electronics 9 (1) (2019) 549–558.

[31] K. Mandal, SBSDS - Stability and Bifurcation of Switched Dynamical System, DSWeb 2019 Tutorials on DS Software Contest, Natick, MA, https://dsweb.siam.org/Software/pager/225/page/4 (November 2019).

[32] P. Kowalyk, A Novel Way of Using Power Modules to Eliminate Electric Vehicle High-Voltage Pre- Charge Circuitry, Vicor Corporation (August 2024).

[33] Flex Power Modules, Selection of Architecture for Systems using Bus Converters and POL Converters, Design Note 023 (December 2017).

[34] P. Davies, T. Curatolo, Redefining Power Delivery Networks with Fixed-Ratio Converters, Vicor Corporation (2020).

[35] L. Benadero, A. El Aroudi, L. Martinez-Salamero, C. K. Tse, Period doubling route to chaos in open-loop boost converters under constant power loading and discontinuous conduction mode conditions, IEEE International Symposium on Circuits and Systems (ISCAS 2020), Seville, Spain, 2020.

[36] L. Benadero, A. El Aroudi, M. Sebastiá-Rullo, H. Valderrama-Blavi, A. Cid-Pastor, L. Martínez-Salamero, Global dynamical analysis of a boost converter with a constant power load and actively damped by a series loss-free resistor, in: Advances in Nonlinear Dynamics and Control of Mechanical and Physical Systems, Springer Nature Singapore, Singapore, 2024, pp. 117–128.

[37] M. Sebastià-Rullo, A. Cid-Pastor, H. Valderrama-Blavi, A. El Aroudi, L. Martínez-Salamero, Series loss-free resistor as stabilizing active damping of constant-power load systems, IEEE Transactions on Circuits and Systems I: Fundamental Theory and Applications, Early access (May 2024).

[38] L. Benadero, A. El Aroudi, L. Martinez-Salamero, C. K. Tse, In-depth analysis of smooth and nonsmooth bifurcations for an open-loop boost converter feeding constant power loads in discontinuous conduction mode, International Journal of Bifurcation and Chaos 33 (04) (2023) 2350043.